Supporting Information

Ultrahigh-Throughput Cross-Flow Filtration of Solution-Processed 2D Materials Enabled by Porous Ceramic Membranes

Santiago Diaz-Arauzo,[a] Julia R. Downing,[a] Daphne Tsai,[a] Jenna Trost,[b] Janan Hui,[c] Kevin Donahue,[d] Nick Antonopoulos,[d] Lindsay E. Chaney,[a] Jennifer B. Dunn,[c] and Mark C. Hersam[a,c,e*]

[a] Department of Materials Science and Engineering, Northwestern University, Evanston, Illinois 60208, United States of America.

[b] Department of Chemical and Biological Engineering, Northwestern University, Evanston, Illinois 60208, United States of America.

[c] Department of Chemistry, Northwestern University, Evanston, Illinois 60208, United States of America.

[d] ALSYS USA, CeraMem, Waltham, Massachusetts 02453, United States of America.

[e] Department of Electrical and Computer Engineering, Northwestern University, Evanston, Illinois 60208, United States of America.

* Corresponding Author: m-hersam@northwestern.edu

1. Section S1. Characterization and Instrumentation

1.1. UV-Vis

A Cary UV-Visible spectrophotometer (Agilent) was used to measure the concentration of graphene in cross-flow filtration (CFF) dispersions. Dispersions were diluted to obtain an absorbance below 1 by using a dilution factor of 1000. Spectra were collected from 300 nm to 800 nm using 1.5 mL plastic cuvettes (Fisher Scientific). Graphene concentration was calculated using the absorbance at a visible wavelength of 660 nm, a molar extinction coefficient (α) of 5000 mL/mg·m, and a path length of 1 cm according to Beer's Law.

1.2. Atomic Force Microscopy

Size analysis of the cross-flow ultrafiltration (CF-UF) retentate streams containing graphene nanosheets was performed via atomic force microscopy using an Asylum Cypher AFM (Oxford Instruments) operated in non-contact tapping mode. CF-UF retentate dispersions were diluted to a concentration of 50 μg/mL with ethanol. 300 nm thick SiO_2/Si wafers were bath sonicated in acetone,

ethanol, and isopropyl alcohol for 5 min each. The diluted dispersion was drop-cast onto the wafers and baked at 350 °C for 30 min to remove any organic residue and ethyl cellulose (EC). A scan area of 2.5 μm × 2.5 μm was used with a scan rate of 0.65 Hz and a resolution of 512 pixels/line. Each scan was manually processed using Gwyddion software to quantify flake dimensions, such as lateral size and thickness. These data were then compiled into histograms and fitted with a log-normal distribution.

1.3. Rotary Evaporation

Exclusively for polymer membrane control experiments, cross-flow microfiltration (CF-MF) permeate and cross-flow ultrafiltration (CF-UF) retentate dispersions were fed into a Buchi rotary evaporator using a condenser temperature of 10°C, a heating temperature of 50°C, and a column pressure at 74 mbar. The holding vessel was rotated at 250 RPM in the heating bath to create turbulent flow and uniform drying, such that the ethanol evaporated from the CFF dispersions and re-condensed in the column. Once the sample was fully dried in this manner, the remaining solids were collected using a sterile plastic spatula and stored.

1.4. Thermogravimetric Analysis

Thermogravimetric analysis (TGA) was used to determine the ethyl cellulose and graphene composition in the powders dried by rotary evaporation. All measurements were taken in a TGA/DSC 3+ instrument (Mettler Toledo) under compressed air (50 mL/min) with a fixed ramp rate (7.5 °C/min) from 25 °C to 600 °C. At 450 °C, after complete EC decomposition, the mass ratio of graphene to ethyl cellulose in the solid powder was calculated by normalizing the remaining mass to the initial sample.

1.5. Ink Formulation and Characterization

CF-UF retentate dispersions produced via cross-flow filtration with polymer membranes were fed into a rotary evaporator to separate graphene/EC solids from ethanol as described in Section S1.3. These rotary-dried powders were dispersed into a 90:10 solution of ethanol:terpineol at a weight loading of 10 g/L for printing. Due to the efficacy of the ceramic membrane, CF-UF retentate dispersions from the integrated CFF process did not require rotary evaporation prior to ink formulation.

CF-UF retentate dispersions from the integrated process were combined with terpineol to produce a 90:10 solution of ethanol:terpineol, yielding an ink with a graphene/EC solids loading of 10 g/L. The dispersions were then bath sonicated for 8 hours to ensure colloidal stability. The resulting dispersion was serially passed through a 3.1 μm nylon syringe filter (Whatman) and then a 1.6 μm nylon syringe filter (Whatman) prior to loading the ink into a commercial aerosol jet printer (Aerosol Jet 200, Optomec). Glass substrates were bath sonicated in acetone, isopropanol, and ethanol for 5 min each before exposure to ozone

plasma at medium power for 2 min. After ink deposition, the printed films were heated in a box furnace to decompose the EC at 350 °C for 30 min.

At the same time, a sample of the ink was collected to perform rheology measurements and acquire viscosity data. These measurements were conducted at room temperature utilizing a Physica MCR 302 rheometer (Anton Paar). The rheometer was equipped with a CP 25-2 fixture, which consisted of a cone-plate fixture with a diameter of 25 mm and a cone angle of 2°. A shear rate sweep was performed from γ =1 s^{-1} to 1000 s^{-1}, and the dynamic viscosity of the ink was recorded at $\gamma = 100$ s^{-1}.

1.6. Raman Spectroscopy

Following EC decomposition, Raman spectroscopy was performed on the aerosol printed films using a LabRAM HR Evolution microscope (Horiba). A 532 nm laser with 10% power was utilized during the spectroscopic analysis. Spectra were acquired using an acquisition time of 30 sec (accumulation = 3), a 2400 g/mm grating, and a laser spot size of 1 μm. The same conditions were applied for analysis of Al_2O_3 membranes.

1.7. Scanning Electron and Optical Microscopy

The morphologies of graphene and graphite particles in aerosol jet printed films, CFF membranes, and drop-casted CFF dispersions were all observed by scanning electron microscopy (SEM) and optical microscopy. For the SEM characterization of ceramic membrane elements, the membrane was cut and polished to obtain a 2 mm x 2 mm x 1 mm piece, which was coated with ≈10 nm of OsO_4 prior to scanning with a SU8030 FEG SEM (Hitachi). Meanwhile, an accelerating voltage of 5.0 kV was used for aerosol jet printed films and drop-casted CFF dispersions. The polished membranes were examined using an accelerating voltage of 2.0 kV. All SEM scans implemented a working distance of ≈4 mm. Finally, a Bruker optical microscope was used with a standard bulb and 20x magnification for lower resolution imaging.

1.8. Electrical Characterization

Following film deposition and thermal decomposition of EC, the thickness of the aerosol jet printed films was measured using a Dektak stylus profilometer equipped with a 5.0 μm stylus radius. Film resistivity was determined by measuring the voltage and current from a probe station (Lucas Labs) in ambient conditions with a Keithley 2400 source meter. To determine the resistivity, the measured thicknesses and voltage-current profiles were inserted into **Equation S1**.

$$\rho = 2\pi \times s \times a \times \frac{V}{I} \times k \tag{S1}$$

where ρ is resistivity, s is the probe spacing (0.04"), a and k are correction factors, and V and I are the voltage and current recorded by the source meter unit, respectively. The correction factor, k, is calculated

from the shortest film length, d, and probe spacing, assuming a 4 mm × 4 mm square in the measurement area according to **Equation S2**, such that $d/s = 1$ and $k = 0.13$.

$$k = \frac{1}{1+\frac{4.54957}{\left(\frac{d}{s}\right)^{1.83824}}}$$ (S2)

To determine sheet resistance, **Equation S3** is employed, with a value of $a = 4.53$ used for thin films. In addition, the film conductivity is determined using **Equation S4**, which utilizes the thickness measurement obtained from stylus profilometry (t).

$$R_s = a \times \left(\frac{V}{I}\right) \times k$$ (S3)

$$c = \frac{1}{R_s \times t}$$ (S4)

2. **Section S2.** Membrane, Flow, and Material Properties of the CFF Processes

We employed two distinct CFF processes with graphene dispersions at the pilot-scale (2.5 L) as described in the main text: one was performed using a polymer membrane element (Table S1) and the other with a ceramic membrane element (Table S2).

Table S1. Pilot-scale polysulfone membrane, flow, and mass transfer attributes for CFF graphene inks.

	Parameter	Value
Membrane Characteristics	Material	Polysulfone
	Fiber Length	31.8 cm
	Inner Diameter	0.75 mm
	Membrane Area	0.16 m^2
	Number of Fibers	300
Flow Characteristics	Tank Volume	7570 mL
	Feed Flow Rate	3785 – 9462 mL/min
	Ambient Pressure	1.0 bar
	Solvent Density	789 kg/m^3
	Viscosity	1.5 cP

Table S2. Pilot-scale ceramic membrane, flow, and mass transfer properties for CFF graphene inks.

	Parameter	Value
Membrane Characteristics	Material	Al_2O_3
	Channel Length	117.8 cm
	Inner Diameter	2.95 mm
	Membrane Area	0.34 m^2
	Number of Channels	31
Flow Characteristics	Tank Volume	7570 mL
	Feed Flow Rate	9462 – 26498 mL/min
	Ambient Pressure	1.0 bar
	Solvent Density	789 kg/m^3
	Viscosity	1.5 cP

A distinguishing attribute of the two processes is the operating windows of graphene concentration and transmembrane pressure during microfiltration (Figure S1). Meanwhile, during ultrafiltration, the graphene content in the retentate increases monotonically with time (Figure S2).
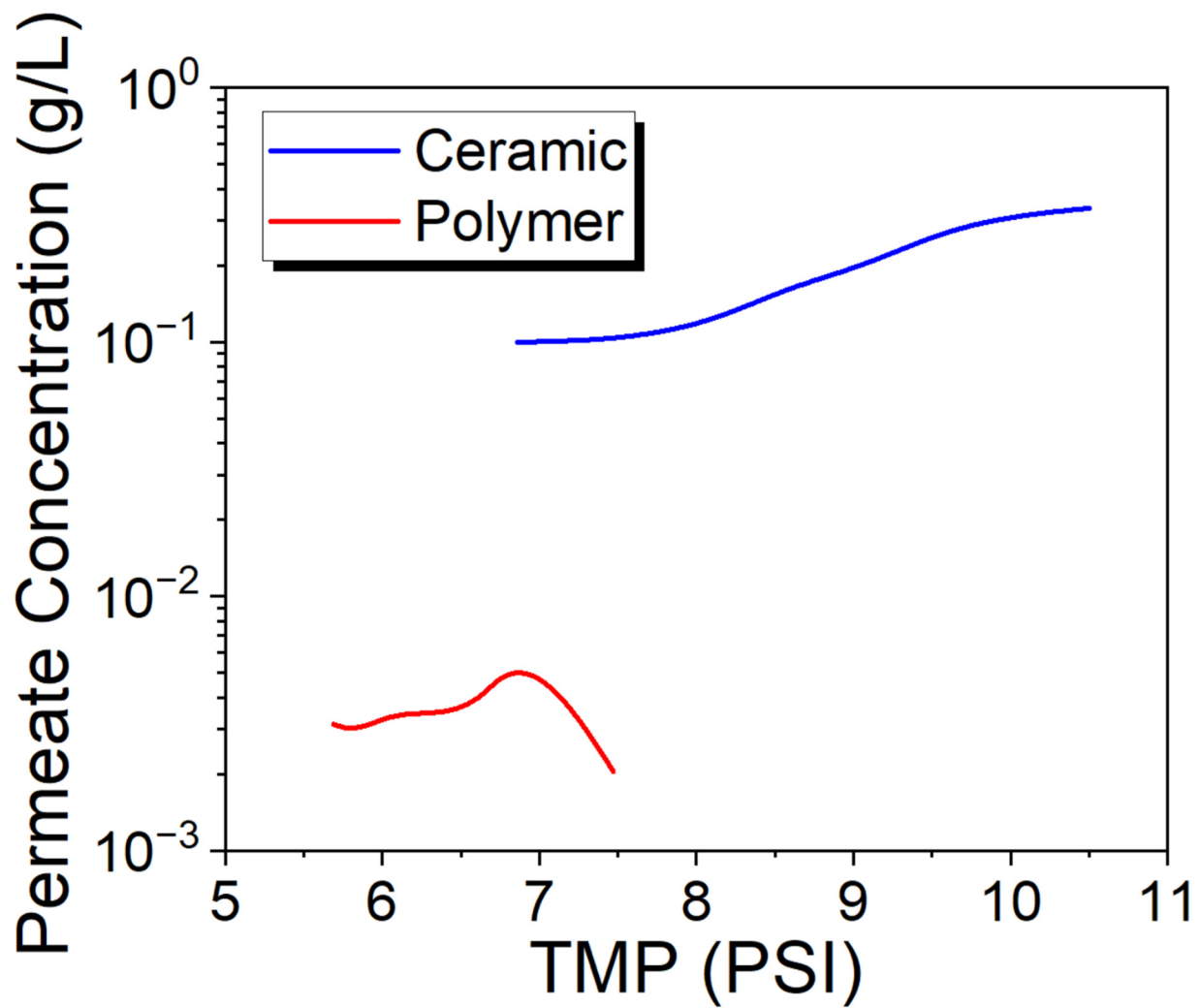
Figure S1. Effect of transmembrane pressure (TMP) on permeate concentration across the CF-MF apparatus using ceramic and polymer membranes.
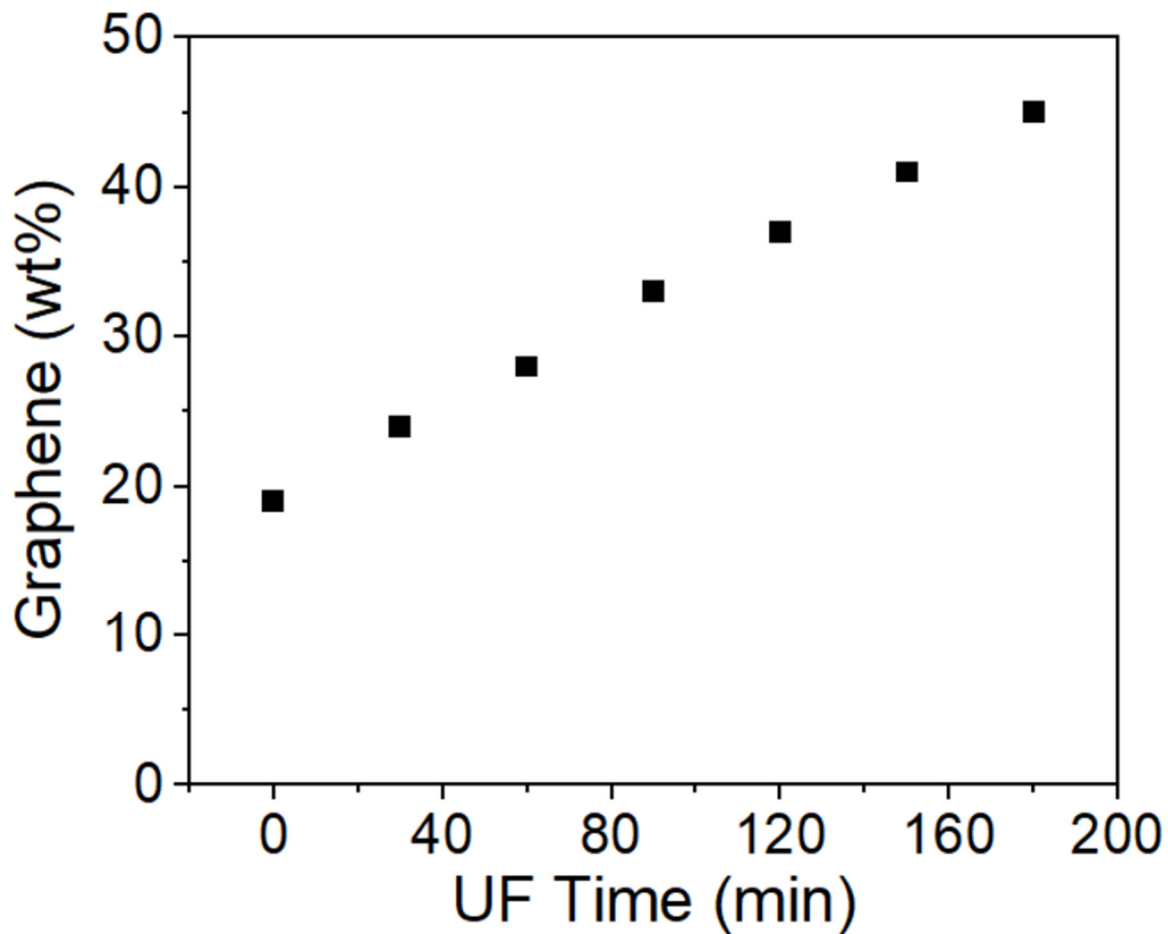
Figure S2. Graphene/EC mass composition with respect to ultrafiltration (UF) time.

The cross-flow ultrafiltration process involves the concentration of the graphene dispersion by filtering ethanol and ethyl cellulose through a nano-porous membrane. To determine the removal of ethyl cellulose (EC), we collected aliquots from the CF-UF retentate at 30 min intervals. Here, we operated in the diafiltration mode of CFF, where pure ethanol was added once a threshold volume was reached. These aliquots were dried, and the resulting powders were analyzed using a thermogravimetric analyzer. Our observations revealed that the graphene fraction increased by 4-5% every 30 min, eventually reaching a mass ratio of 1:1 graphene:EC (Fig. S2). This finding is significant since it indicates the ability of the process to fine-tune the graphene:EC composition, which is crucial for various additive manufacturing printing techniques.

After CF-MF and prior to ink formulations, the various processes were characterized via Raman Spectroscopy (Figure S3). Note that the CF-MF permeate and CF-UF retentate are compositionally identical. In comparison to graphene produced from polymer membranes, the Raman peaks from ceramic

membranes are similar.[3] Both spectra show a D peak at ≈1350 cm^{-1}, a G peak at ≈1620 cm^{-1}, and a 2D peak at ≈2700 cm^{-1}.
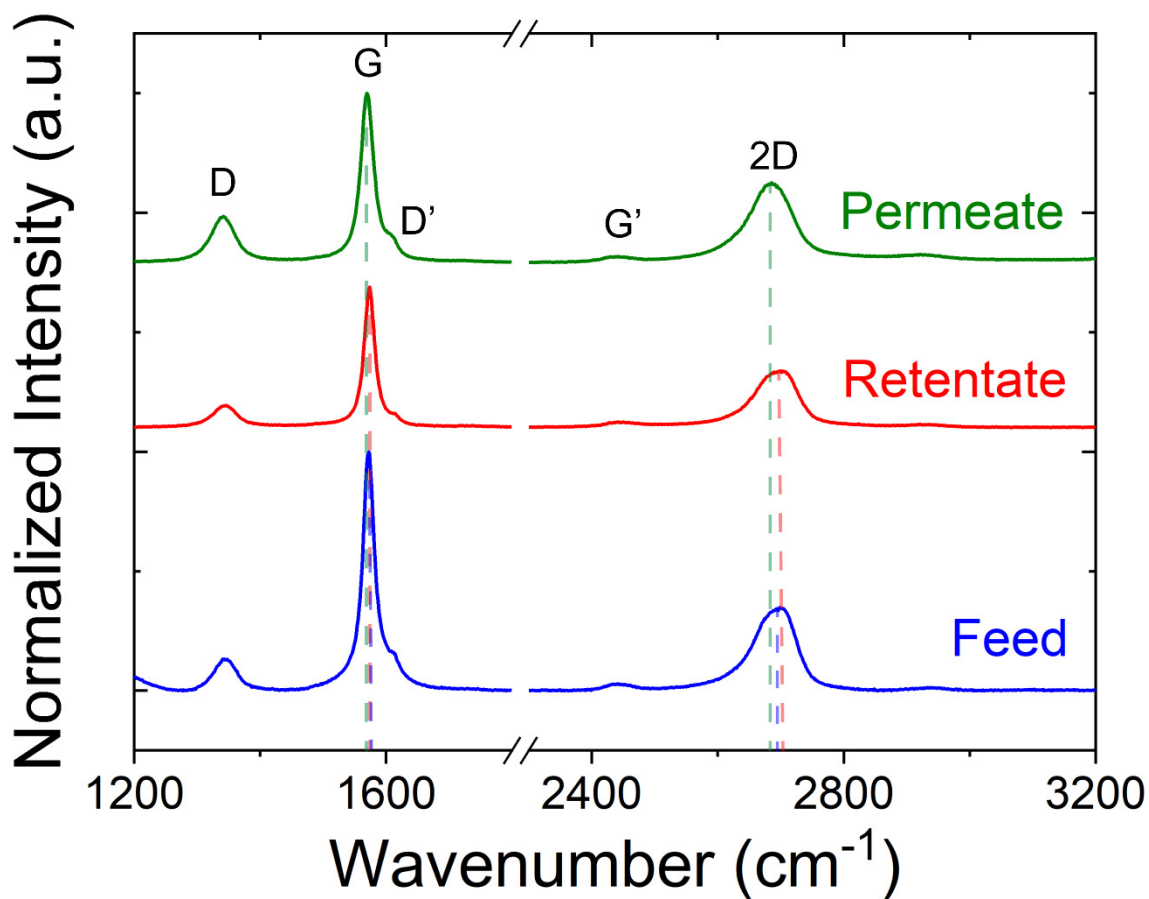

Figure S3. Raman spectroscopy of drop-cast CF-MF feed, retentate, and permeate dispersions.

Next, the CF-MF permeate/CF-UF retentate dispersions were formulated into printable inks. The viscosity of these process streams is benchmarked against the as-exfoliated dispersion from a wet jet milling apparatus (WJM) and the pure ethanol solvent (Figure S4). Viscosity for the final printable ink formulation is depicted in Figure S5.

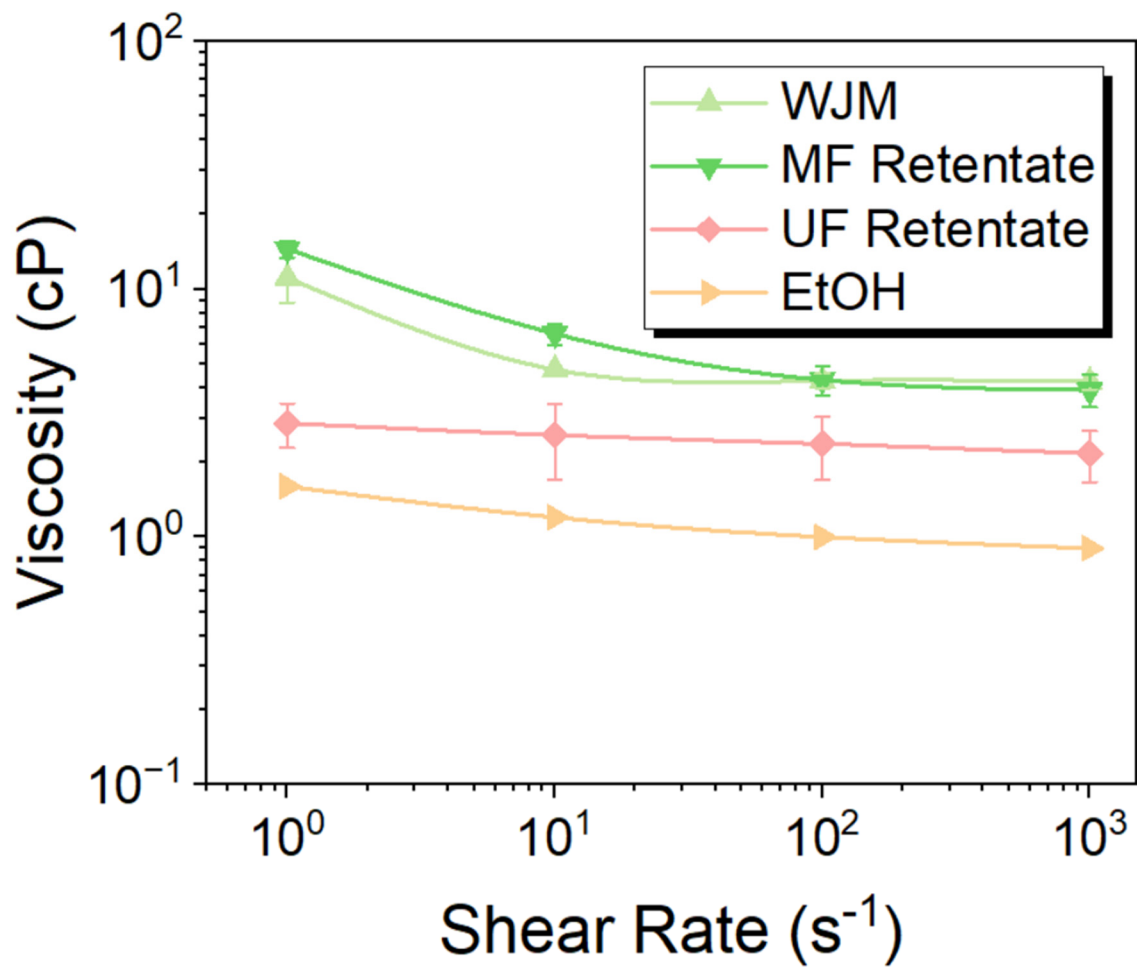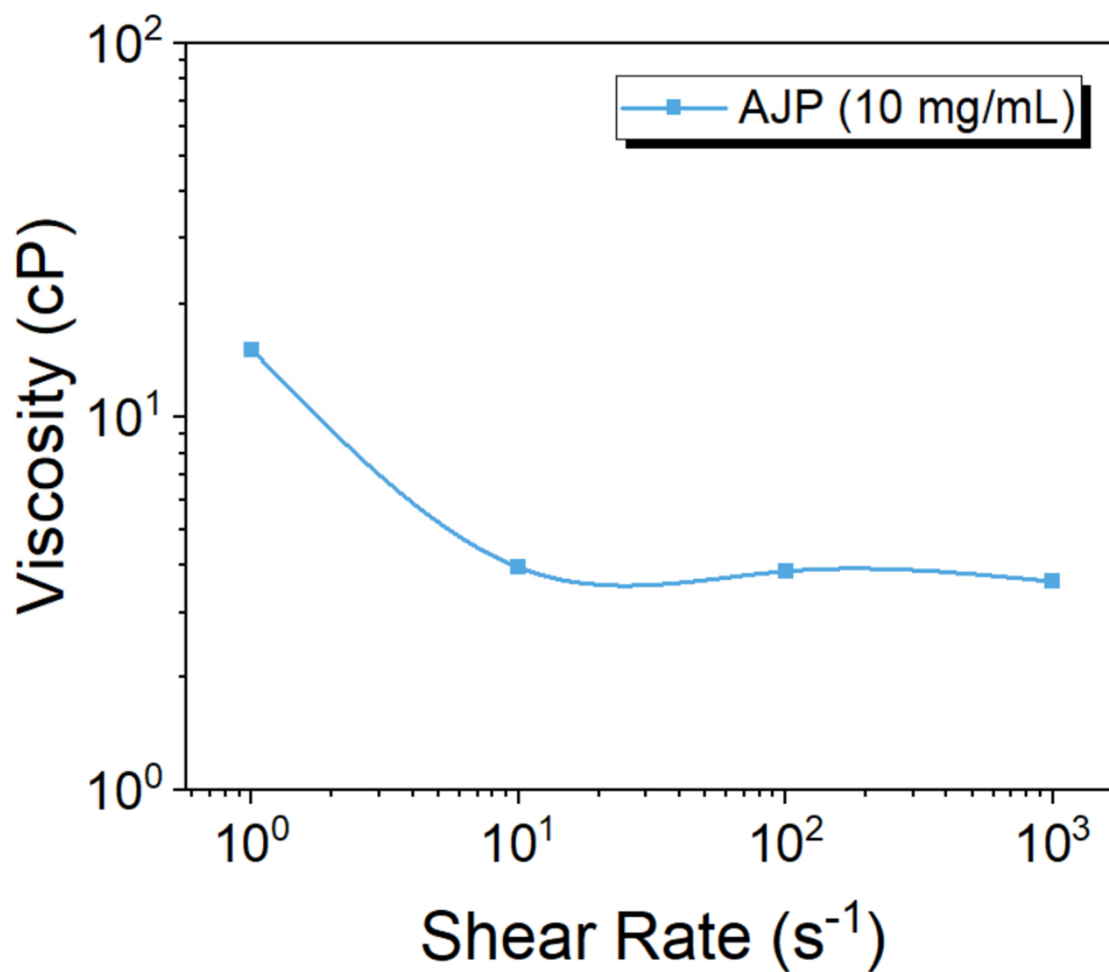**Figure S4.** Viscosity curves of the dispersions across the manufacturing process.

Figure S5. Viscosity curve of the AJP ink.

The overall throughput of our CFF process is benchmarked against prior demonstrations of nanomaterial CFF in Figure S6 and Table S3.
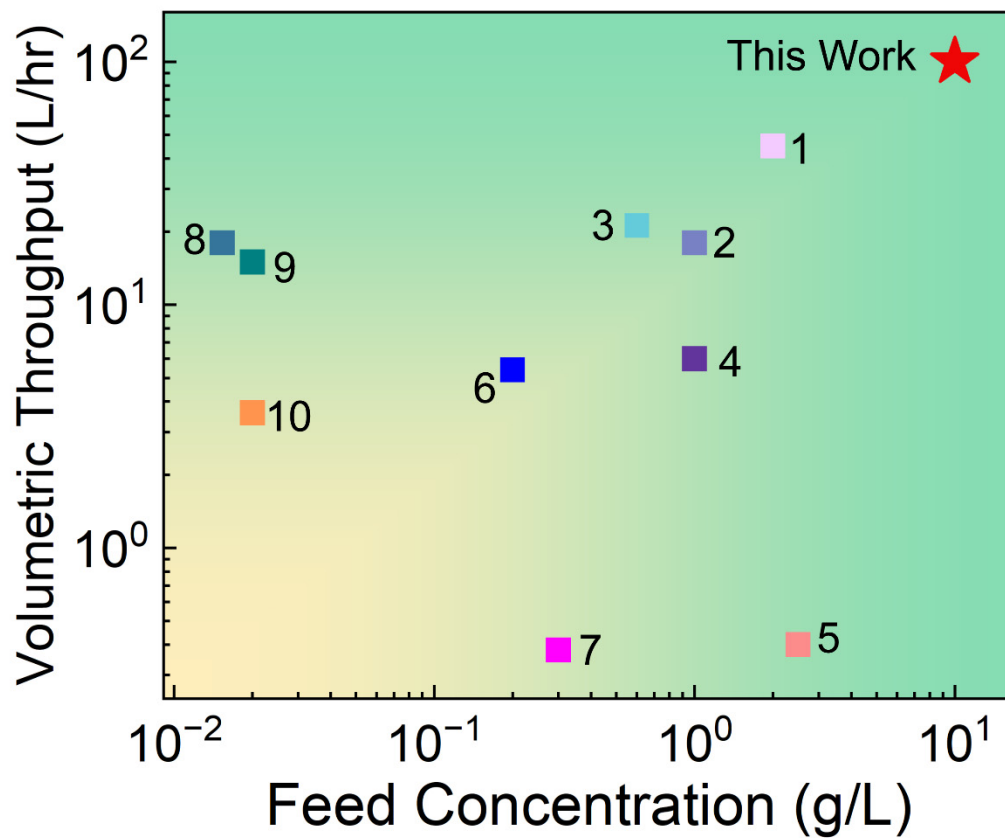
Figure S6. Volumetric throughput comparison of the integrated CFF process in comparison to alternative CFF-processed nanomaterials.

Supplementary Table S3: Comparison of various cross-flow filtration methods for nanomaterials.

Reference	Membrane Material	Nanomaterial	Feed Concentration (g/L)	Mass Throughput (g/hr)	Volumetric Throughput (L/hr)
[S1]	Stainless steel support and alumina ceramic	Graphene Oxide	2	90	45
[S2]	Krosflow Midi module	Silver Nanoparticles	0.0153	0.28	18
[S3]	Polysulfone	Graphene	0.6	12.72	21.2
[S4]	Polycarbonate/ Polyethersulfone	Cellulose Nanocrystals	1	6	6
[S5]	Polysulfone	Gold Nanoparticles	2.5	1	0.4
[S6]	MicroKros HF Modules	Silver Nanowires	0.2	1.08	5.4
[S7]	Polyacrylonitrile	Bentonite	0.3	0.11	0.38
[S8]	Stainless steel support and alumina ceramic	Graphene Oxide	1	18	18
[S9]	Disc Track-Etched Membranes	Graphene Quantum Dots	0.02	0.30	15
[S10]	Hydrophilic Polytetra-fluoroethylene	Carbon Nanotubes	0.02	0.07	3.6
This Work	Ceramic-based oxide	Graphene	10	1000	100

3.   Section S3. Assumptions, Supplementary Values, and Sensitivity Analyses for LCA.

As described in the main text, life cycle analysis (LCA) and technoeconomic analysis (TEA) were applied to the incumbent CFF process for graphene with polymer membranes and compared against the present exfoliation-to-print CFF process with ceramic membrane elements. The following sections detail those analyses and associated inputs. In order to provide a strong comparison between the two processes, we included the ink formulation process that was not included in our previous study.[S3]

3.1.   Materials and Consumables

Each process considered graphite, EC, and ethanol as inputs into the size refinement and ink formulation sub-processes. Mass ratios of graphite, EC, and ethanol inputs are consistent in both processes. **Figure 4a** of the main text illustrates the system boundary. **Table 1** illustrates the lifecycle inventory (LCI) for 1 L of graphene ink. In the polymer membrane separation process, ink formulation involves the use of a rotary evaporation, whereas the ceramic membrane separation process eliminates the need for a rotary evaporator. This difference is attributed to the higher concentration of the graphene dispersion in the ceramic membrane process, which allows for the direct production of a sufficiently concentrated ink for printing. Conversely, the polymer membrane process lacks the capability to produce such a concentrated ink and thus requires the use of rotary evaporation to collect and redisperse the solids to produce a concentrated ink.[S3] All graphene yields and concentrations were confirmed using a UV-Vis spectrometer.

Based on our empirical observations, we estimated the need for 20 polymer membranes since the average lifetime for a polymer membrane is ≈18 days, whereas we assumed the need for 10 ceramic membranes since the average lifetime for a ceramic membrane is ≈36 days. For this analysis, we assume that the polymer membrane study requires 1.5 hours of labor per run, whereas the ceramic membrane study requires 1 hour of labor per run largely due to the additional cleaning steps required for the polymer membrane. The labor required for ink formulation is the same in both processes.

Polypropylene tubing, membrane elements, and glass bottles were considered as consumables for both processes. The polymer membrane process considered polysulfone as a membrane material, and the ceramic membrane size refinement process considered oxide-based ceramics as membrane materials. In order to determine the LCA impacts for the production of these membranes, we utilized the impacts calculated from polysulfone and bauxite production within Greenhouse Gases, Regulated Emissions, and Energy Use in Transportation Model (GREET) models.[S11]

3.2.   Equipment

Equipment was determined from **Figure 4a** in the main text. In our analysis, we assumed an overall process lifetime of 20 years. All equipment (sensors, pumps, rotary evaporator, etc.) lifetimes were

determined from consultations with manufacturers and official manuals. The equipment prices were obtained from manufacturer quotations at the time of purchase and subsequently recalculated to account for inflation in 2023.

3.3. Volumetric Throughput and Recycling

The volumetric throughput of the polymer membrane size refinement and ink formulation process was calculated by determining the volume of dispersion processed within the operating time in both the CF-MF and CF-UF processes. The throughput of the integrated ceramic membrane size refinement process was determined by determining the volume of dispersion within solely the integrated CF-MF/CF-UF process. In order to convert to mass throughput, we multiplied the volumetric throughput with the feed concentration, similar to previous reports.[S1-S10]

In order to consider the effects of recycling on the LCA, the rotary evaporator was used to recycle solids and liquids solely within the polymer membrane size refinement process. Specifically, graphite can only be recovered from the CF-MF retentate using the rotary evaporator. EC and ethanol can be recovered via the CF-MF permeate and CF-UF permeate. Additionally, EC and ethanol are recovered from the CF-UF retentate stream exclusively within the polymer membrane size-refinement process. Therefore, all of the ethyl cellulose, ethanol, and nearly all of the unexfoliated graphite was recovered with polymer membranes and rotary evaporation.

However, the CF-UF retentate from the ceramic membrane process serves directly as the ink. In order to recycle graphite, EC, and ethanol from the ceramic membrane process, we exclude the rotary evaporator and process the dispersion directly by feeding them into the wet jet milling instrument. With ceramic membranes, we recycle unexfoliated graphite, EC, and ethanol.

Completing the TEA and LCA required us to calculate the time required for the rotary evaporation process when the membrane in the process is polymeric. Within the ceramic membrane process, we found that the CF-MF retentate and CF-UF permeate can avoid the rotary evaporation step altogether. We determined that the evaporation of any dispersion has a rate of 500 mL/0.5 hr = 1 L/hr. The glass bottles within the ink formulation process were recycled for both processes.

3.4. Electricity Demand

From the equipment manuals for the pumps and rotary evaporator, we determined the maximum rated current draw for each tool. We estimated the electricity consumption for each equipment by scaling power consumption based on active run time (i.e., the equipment is not using the full power consumption throughout the course of the entire operation).

3.5. Environmental and Economic Impacts

The environmental and economic impacts for the inputs used to produce graphene inks are summarized in **Table 2** and **Tables S4 and S5**. We utilized the median impact values for graphite production, ethyl cellulose, ethanol, polysulfone filters, and polypropylene reported in our previous study.[S3] The impacts from electricity and ceramic membrane production are derived from GREET.[S11] The polymer size-refinement process can run up to 9 times a day, with 1 hour attributed to the ink formulation step. The ceramic size-refinement process can run up to 20 times a day with 1 hour similarly attributed to the ink formulation step.

Tables S6 – S9 highlight the environmental intensities and economic costs pertaining to the inputs in the polymer size-refinement, ceramic size-refinement, and ink formulation processes. Although quantifying the environmental impact of membrane manufacturing presents challenges, other literature indicates a comparatively lower environmental burden for this stage compared to the rest of the process.[13]

Supplementary Table S4. Environmental and techno-economic parameters.

Parameter	Unit	Value	Reference
CO_2 GWP_{100}	g CO_2-eq/g	1	[S13]
CH_4 GWP_{100}	g CO_2-eq/g	30	[S13]
N_2O GWP_{100}	g CO_2-eq/g	265	[S13]
U.S. Electricity Cost	$/kWh	0.1582	[S14]
U.S. Median Hourly Wage	$/hr	21.83	[S15]
Discount Rate	%	12	–
Process Lifetime	years	20	–

Note: The units above and preceding are expressed per g of graphene. In order to convert from g of graphene to L of graphene ink, we adhered to Equation 1 to convert the gross environmental and economic impact accordingly.

Supplementary Table S5. Techno-economic parameters pertaining to economic performance.

Parameter	Unit	Polymer Membrane Values	Ceramic Membrane Values
Total Processing Time	hr	2.57	1.15
Labor Time	hr	8	8
Runs per day	–	9	20
Runs per year	–	3285	7300
Annual Graphene Yield	kg graphene	14.9	553
Pumps[#]	–	1.14	0.57
Digital Pressure Monitor and Sensors[#]	–	2	1
Rotary Evaporator[#]	–	2	–

[#]These quantities are reflected across a process lifetime of 20 years.

Supplementary Table S6. Fossil energy intensity per kg of input 5 parameters.

Material	Unit	Value	Reference
Graphite	MJ/kg	110	[S16]
Ethanol	MJ/kg	15	[S11]
Ethyl Cellulose	MJ/kg	8.2	[S17]
Terpineol	MJ/kg	14	[S17]
Polymer Membrane	MJ/kg	30	[S18]
Ceramic Membrane	MJ/kg	16	[S11]
Tubing (Silicone)	MJ/kg	109	[S11]
Glass	MJ/kg	13	[S11]
Electricity	MJ/MJ	1.3	[S14]

Supplementary Table S7. Carbon intensity per kg of input.

Material	Unit	Value	Reference
Graphite	g/kg	3500	[S16]
Ethanol	g/kg	1461	[S11]
Ethyl Cellulose	g/kg	330	[S17]
Terpineol	g/kg	44	[S17]
Polymer Membrane	g/kg	13	[S18]
Ceramic Membrane	g/kg	56	[S11]
Tubing (Silicone)	g/kg	11709	[S11]
Glass	g/kg	16	[S11]
Electricity	MJ/MJ	1.3	[S14]

Supplementary Table S8. Water consumption per kg of input.

Material	Unit	Value	Reference
Graphite	kg/kg	41	[S16]
Ethanol	kg/kg	40	[S11]
Ethyl Cellulose	kg/kg	25	[S17]
Terpineol	kg/kg	20	[S17]
Polymer Membrane	kg/kg	29	[S18]
Ceramic Membrane	kg/kg	1.5	[S11]
Tubing (Silicone)	kg/kg	45	[S11]
Glass	kg/kg	0.41	[S11]
Electricity	MJ/MJ	1.3	[S14]

Supplementary Table S9. Total cost of material inputs per kg of input.

Material	Unit	Value	Reference
Graphite	$/kg	23	[S16]
Ethanol	$/kg	4.7	[S11]
Ethyl Cellulose	$/kg	988	[S17]
Terpineol	$/kg	157	[S17]
Polymer Membrane	$/kg	5144	–
Ceramic Membrane	$/kg	416	–
Tubing (Silicone)	$/kg	212	–
Glass Bottle	$/kg	35	[S11]

Note: Tubing and membrane costs were determined by the most recent quote provided by vendors with a university discount.

Table S10 summarizes the results from the technoeconomic analysis pertaining to amortized capital cost, consumables, electricity, and labor. While the primary text provided the overall capital and operating costs associated with producing 1 L of graphene ink over the lifespan of the process, our aim was to evaluate the major factors influencing our various costs. For example, while the amortized capital cost captures the costs associated with equipment, we noticed significant contributors from electricity and labor in the polymer membrane separation process. By removing the rotary evaporator in the second process and incorporating an integrated separation and concentration process using ceramic membranes, we reduce all related non-material capital and operating costs by at least 97%.

Supplementary Table S10. Techno-economic impacts ($) per L of graphene ink.

	ACO[‡]	Consumables	Electricity	Labor	Total
Polymer Membrane	174	36	66	73	349
Ceramic Membrane	5.4	0.33	2.2	2.9	11

[‡]ACO = amortized capital cost, which is defined as the total operating cost for equipment divided by the mass throughput.

3.6.   Sensitivity Analyses Relating to Fouling, Labor, and Ethanol Consumption on LCA/TEA

To address the potential effects of membrane fouling on TEA and LCA results, we conducted a sensitivity analysis using two scenarios: (i) doubling the membrane inventory in both processes; (ii) increasing the cleaning time by 50%. We argue that these two scenarios are possible responses to increased fouling in the CFF process. We solely considered the active run time of the machine to draw the fairest comparison possible, thereby excluding downtime or time required for cleaning. Initially, we observed a small decrease of ≈1% in throughput since the membrane requires a cleaning step at the start of operation and at the end of the day. For the first case, we observed a change of <0.001% increase across all three environmental impacts. The cause for such a negligible response is attributable to the mass of the membrane (≈5 kg) across one year of processing in comparison to the mass throughput (>1500 kg graphite and ethanol) of raw inputs. The TEA shows an improvement of 2% in cost reduction as a result of the inexpensive cost of the ceramic membrane (≈$700) in comparison to the more costly polymer membrane (≈$1500). In regard to the second case, we observed a negligible ($<10^{-3}$ %) response across all three environmental impacts as a result of the minimal power draw that stems from the pumps. We observed an improvement of 1% in cost reduction as the labor required decreased since fewer runs were available due to the increase in cleaning.

Secondly, we performed a sensitivity analysis on the effect of manual labor within our TEA calculations. We focused on increasing the amount of manual labor required within a day by adjusting the overall labor time by 225%. This estimate included changing the labor requirements in the size-refinement and ink formulations processes proportionally – i.e., labor time for ink formulation changed from 10 min to 22.5 min, whereas labor time for processing changed from 1 hr to 2.25 hours. We observed < 0.3% change in environmental impacts, stemming from the reduction in number of resources (electricity and materials) and throughput. On the other hand, we saw a 4% improvement in cost reduction between both processes as the specific production cost for the polymer membrane process increased from $180.39/L of ink to $292.04/L of ink, whereas for the ceramic membrane process, the change was ≈$4/L of ink. This change is primarily due to the increased amortized capital cost – i.e., the total cost for labor, consumables, and electricity with respect to throughput of each process ($285/L of ink compared to $9/L of ink).

Lastly, in order to better understand the strong environmental impact of ethanol, we increased the ethanol required for our overall processes by 50%. Here, we observed an increase of 1–3 % in environmental impacts. We argue that increasing the amount of ethanol has less impact on the ceramic membrane separation and ink formulation process due to the higher throughput relative to the polymer membrane size-refinement approach. Moreover, recycling ethanol in the polymer membrane approach requires additional rotary evaporation time which increases electricity draw, GHG emissions, and fossil fuel and water consumption.

In summary, from the results in **Table 1**, we observed that electricity, ethanol, terpineol were significant contributors to greenhouse gas emission, fossil fuel consumption, and water consumption. Full automation, movement towards aqueous-based solvents, and sourcing sustainable electricity could further reduce the overall impact from both processes. The results from **Table 3** demonstrate that consumables, labor, and equipment costs are the primary contributors to costs and expenses. Increasing the lifetime of equipment and reducing the number of consumables would potentially lower the expenses in TEA. Moreover, full automation would nullify labor costs and increase the overall safety of the process.

3.7.   Detailed Energy Usage Breakdown of Equipment for Polymer and Ceramic Membranes

In order to understand the energy usage and emissions produced from our process overall, we tabulate the electricity required for 1 run. For polymeric membranes, this process includes the equipment involved in microfiltration, ultrafiltration, and rotary evaporation. Ceramic membranes include only microfiltration and ultrafiltration.

Supplementary Table S11. Life cycle analysis inputs of each process in the polymeric membrane study.

	Electricity (kWh)
Microfiltration	0.43
Ultrafiltration	0.11
Rotary Evaporation	2.7

Supplementary Table S12. Life cycle analysis inputs of each process in the ceramic membrane study.

	Electricity (kWh)
Microfiltration	0.09
Ultrafiltration	0.002

Polymer membranes necessitate longer running times to produce 1 L of graphene ink as a result of the dilution required for effective cross-flow filtration. In contrast, ceramic membranes necessitate minimal dilution and do not require rotary evaporation, which drastically influence the electrical usage per 1 L of graphene ink. Lastly, recycling via rotary evaporation is energy-intensive due to the time required for evaporation, especially as the process scales towards multiple iterations.

References

1. Y. Shi, X. Ye, L. Shen and N. Bao, *Chem. Eng. Sci.*, 2021, **248**, 117143.

2. J. C. Trefry, J. L. Monahan, K. M. Weaver, A. J. Meyerhoefer, M. M. Markopolous, Z. S. Arnold, D. P. Wooley and I. E. Pavel, *J. Am. Chem. Soc.*, 2010, **132**, 10970–10972.

3. J. R. Downing, S. Diaz-Arauzo, L. E. Chaney, D. Tsai, J. Hui, J. T. Seo, D. R. Cohen, M. Dango, J. Zhang, N. X. Williams, J. H. Qian, J. B. Dunn and M. C. Hersam, *Adv. Mater.*, 2023, **35**, 2212042.

4. F. Pignon, E. F. Semeraro, W. Chèvremont, H. Bodiguel, N. Hengl, M. Karrouch and M. Sztucki, *J. Phys. Chem. C*, 2021, **125**, 18409–18419.

5. S. F. Sweeney, G. H. Woehrle and J. E. Hutchison, *J. Am. Chem. Soc.*, 2006, **128**, 3190–3197.

6. K. C. Pradel, K. Sohn and J. Huang, *Angew. Chem. Int. Ed.*, 2011, **50**, 3412–3416.

7. P. Bílek and F. Wicaksana, *EPJ Web Conf.*, 2022, **269**, 01004.

8. C. Li, Y. Guo, L. Shen, C. Ji and N. Bao, *Chem. Eng. Sci.*, 2019, **200**, 127–137.

9. S.-G. Yim, Y. Kim, Y.-E. Kang, B. Moon, E. Jung and S. Yang, *Nanomaterials*, 2018, **8**, 959.

10. S. Ohmori, T. Saito, B. Shukla, M. Yumura and S. Iijima, *ACS Nano*, 2010, **4**, 3606–3610.

11. Argonne National Laboratory. GREET 2020. https://greet.es.anl.gov/index.php (accessed July 2023).

12. X. Wang, A. Anctil and S. J. Masten, *Environ. Eng. Sci.*, 2019, **36**, 149–157.

13. Core Writing Team, R.K. Pachauri and L.A. Meyer (eds.) in *Climate Change 2014: Synthesis Report. Contribution of Working Groups I, II, III to the Fifth Assessment Report of the Intergovernmental Panel on Climate Change*, IPCC, Geneva, Switzerland 2015.

14. Average Energy Prices, Chicago-Naperville-Elgin — October 2021: Midwest Information Office: U.S. Bureau of Labor Statistics. https://www.bls.gov/regions/midwest/news-release/averageenergyprices_chicago.htm. (accessed July 2023).

15. Chicago-Naperville-Elgin, IL-IN-WI - May 2020 OEWS Metropolitan and Nonmetropolitan Area Occupational Employment and Wage Estimates. https://www.bls.gov/oes/current/oes_16980.htm, (accessed July 2023).

16. S. W. Gao, X. Z. Gong, Y. Liu and Q. Q. Zhang, *Mater. Sci. Forum*, 2018, **913**, 985–990.

17. J.-A. Alberola-Borràs, J. A. Baker, F. De Rossi, R. Vidal, D. Beynon, K. E. A. Hooper, T. M. Watson and I. Mora-Seró, *iScience*, 2018, **9**, 542–551.

18. P. Yadav, N. Ismail, M. Essalhi, M. Tysklind, D. Athanassiadis and N. Tavajohi, *J. Membr. Sci.*, 2021, **622**, 118987.